

Fidelity bounds for spin-dependent kicks with pulsed lasers

C. Sagaseta^{1,*}, H. Liu², V. D. Vaidya², C. R. Viteri², J. J. García-Ripoll³ and E. Torrontegui^{1,*}

¹Department of Physics, Universidad Carlos III de Madrid, Avenida de la Universidad 30, 28911 Leganés, Madrid, Spain

²IonQ, Inc., 4505 Campus Drive, College Park, MD 20740, USA

³Instituto de Física Fundamental, Consejo Superior de Investigaciones Científicas (IFF-CSIC), Calle Serrano 113b, 28006 Madrid, Spain

*Authors to whom any correspondence should be addressed.

E-mail: csagaset@fis.uc3m.es, eriktorrontegui@gmail.com

Keywords: spin-dependent kick, fast gates, trapped ions, quantum computing

Abstract

Excitation of trapped-ion hyperfine qubits with fast optical Raman pulses enables faster-than-trap-period entangling gates with qubits of long coherence time for practical quantum computation. Achieving high-fidelity fast two-qubit gates requires high-quality spin-dependent kicks (SDKs), which form their fundamental building blocks. Here, we characterize the control parameters (including Raman frequency difference, pulse arrival times, Lamb–Dicke parameter, temperature, pulse width, and SDK time) that maximize the performance of single-ion SDKs for protocols compatible with performed experiments involving a small number of fast pulses. We demonstrate through analytical methods and numerical simulations that, within the model commonly used for infidelity optimization, finite pulse duration is the dominant source of error, exceeding the contribution of secular motion by orders of magnitude for nanosecond-scale SDKs. Low infidelities—below 10^{-3} for schemes with $\gtrsim 10$ fixed-amplitude, equispaced, picosecond pulses—are achievable in SDK times on the order of nanoseconds. These results provide quantitative design rules for achieving competitive SDK fidelities with current pulsed-laser technology, laying the foundation for sub-microsecond trapped-ion quantum entangling operations.

1 Introduction

Trapped ions are a leading platform for quantum information processing [1]. Qubits encoded in internal electronic states exhibit extremely long coherence times [2, 3] and can be manipulated with high precision using electromagnetic fields [4]. Among all quantum computing platforms, trapped ions currently achieve record fidelities for state preparation and measurement [5], as well as for single-qubit [6] and two-qubit gates, both electronic and laser-based [7, 8]. These capabilities have enabled demonstrations of quantum error correction [9, 10, 11, 12, 13] and the implementation of small-scale quantum algorithms [14, 15, 16, 17, 18].

Most quantum gates in trapped-ion systems operate on adiabatic timescales with respect to the motional dynamics of the ions, since they rely on spectroscopically resolving individual modes of motion [19]. As the number of ions increases, gate operations become more difficult to realize due to normal-mode crowding and unwanted couplings [20, 21, 22], effectively imposing a speed threshold for achieving high fidelity.

In terms of scalability, the dominant architecture is the quantum charge-coupled device (QCCD) [23, 24], which combines small ion registers with ion transport between functional zones. This scheme allows the record fidelities achieved in the smallest processors to be approached while scaling system size [25]. Connectivity can be provided either by shuttling ions between devices [24, 26] or by linking them through photonic interconnects [27, 28, 29, 30, 31, 32, 33]. However, in such modular architectures the dominant speed bottleneck arises from ion transport, as the ions must be moved and subsequently recooled before gate operations can be performed [34].

Fast gates provide an alternative approach to overcoming the scalability–speed trade-off while maintaining the required high fidelity [35, 36, 37]. In these schemes, broadband laser pulses impulsively excite the ions to generate spin–motion entanglement without requiring cooling to the Lamb–Dicke regime [38, 39], enabling two-qubit gates on timescales faster than the motional periods of the ions [40]. Theoretical studies further show that fast two-qubit gates can be

performed with high fidelity between arbitrary pairs of ions in a long chain [41, 42, 43, 44, 45, 46], potentially reducing resource overhead in modular architectures implementing fast gates.

These fast gates are engineered through sequences of spin-dependent kicks (SDKs) [40, 47], which couple the ion spin and momentum degrees of freedom: a spin flip is accompanied by a momentum change whose sign depends on the spin state. The performance of fast two-qubit gates depends directly on the quality of individual SDKs, though agnostic to the specific SDK implementation, so achieving high-fidelity kicks is paramount [46]. Precursor studies established the underlying mechanism and the ideal conditions required to generate a SDK using pulsed lasers [38, 40]. While fast single-qubit [48, 49] and two-qubit gates [47] have been demonstrated, the parameter regimes needed to create SDKs with pulsed protocols have been derived under three approximations—high-pulse number trains, instantaneous pulses, and negligible ion motion [38, 40]—which limit the fidelities achievable under realistic experimental conditions [47].

For improved quantum computing performance, it is desirable to have protocols with a small number of pulses [38, 47, 50] to shorten SDK times and minimize the impact of low-frequency noise. This motivates studying the optimal conditions for few-pulse protocols and characterizing the errors that arise when finite pulse width and ion motion are included in the model, thereby providing more realistic fidelity limits. To address these questions, we follow a bottom-up approach, where we first identify the optimal parameters in the idealized model for a small number of pulses and then sequentially relax each approximation to study their impact on the infidelity.

This work achieves theoretical characterization of all relevant aspects that influence on SDK performance, namely Raman frequency difference, repetition time between pulses, Lamb–Dicke parameter, temperature, pulse width, and SDK time. We show that low infidelity—below 10^{-3} for protocols with $\gtrsim 10$ fixed-amplitude, equally-spaced, picosecond pulses—is attainable in SDK times of a few nanoseconds. A longer pulse width significantly impacts the SDK protocol, highlighting the importance of considering it in parameter optimization. In contrast, we find that ion secular motion has a small effect during the few-nanosecond-long SDK, with an error of the order of 10^{-5} .

The manuscript is organized as follows. Sec. 2 presents the model and the pulsed protocol used to create a SDK. Sec. 3 deals with protocols composed of a small number of delta pulses exciting a non-moving ion, and the optimization of parameters to maximize the SDK process. In Sec. 4 we find the error caused by considering the finite duration of the pulses, while in Sec. 5 we analyze the impact of the ion motion on the SDK protocol. Conclusions and outlook are given in Sec. 6.

2 Model

2.1 Raman-illuminated trapped ion

We consider a single ion in a harmonic potential interacting with two Raman beams. The qubit is encoded in the ground-state hyperfine levels and the Raman beams arrive from counter-propagating directions along x with orthogonal linear polarizations (lin \perp lin), both orthogonal to an applied static magnetic field defining the quantization axis; see Fig. 1(a). This polarization configuration produces a polarization gradient at the position of the ion, which couples spin and motion [51]. Assuming that the pulses from each beam have the same envelope and they arrive simultaneously at the ion, the effective Hamiltonian in the RWA after adiabatically eliminating the excited states is given by ($\hbar = 1$) [38, 40]

$$\hat{H} = \underbrace{\omega_t \hat{a}^\dagger \hat{a}}_{\hat{H}_t} + \underbrace{\frac{\omega_{\text{hf}}}{2} \hat{\sigma}_z}_{\hat{H}_{\text{hf}}} + \underbrace{\mathcal{W}(t) \sin(k_d \hat{x} + \delta t + \varphi_0) \hat{\sigma}_x}_{\hat{H}_{\text{int}}(t)}, \quad (1)$$

where \hat{a}^\dagger (\hat{a}) is the creation (annihilation) operator of the motional mode, $\hat{\sigma}_x$ and $\hat{\sigma}_z$ are the Pauli matrices, ω_t is the trap frequency, ω_{hf} is the hyperfine qubit frequency, $\mathcal{W}(t)$ is the beam envelope, $k_d = k_1 - k_2$ is the difference wavenumber of the counter-propagating beams, δ is the frequency difference between the beams and φ_0 is an initial phase. Equation (1) is valid as long as $\Delta \gg \omega_{\text{hf}}$ (see Fig. 1(b)) and $\tau \partial_t \mathcal{W}(t) \ll \Delta$, where τ is the pulse duration. Also, the bandwidth of $\mathcal{W}(t)$ must be much larger than ω_{hf} to be able to resolve the qubit splitting, but much smaller than Δ to avoid exciting any higher level. We describe the state of the ion by the computational basis of the qubit $\{|Q\rangle\}$, with $Q \in \{0, 1\}$, times the Fock basis $\{|f\rangle\}$, with $f \in \mathbb{N}_0$.

2.2 Spin-dependent kicks

We follow the scheme with counter-propagating trains of short pulses, as depicted in Fig. 1(a), proposed by Mizrahi *et al.* [38, 40] to produce a SDK. The requirements for achieving this were derived taking three approximations: (i) the number of pulses is large, $N \rightarrow \infty$; (ii) the pulse

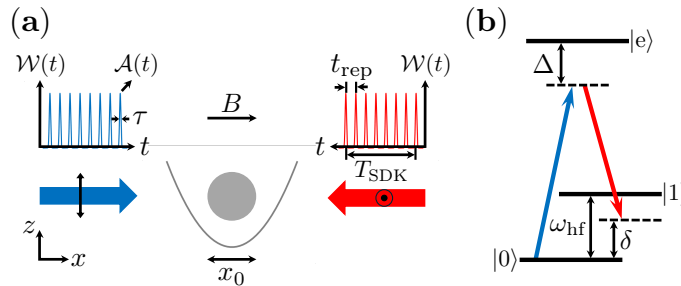


Figure 1. Schematic of the pulsed Raman SDK. Two counter-propagating beams in the lin \perp lin polarization configuration interact with a single ion (grey ball) confined in a harmonic potential (grey parabola) with characteristic length x_0 , that corresponds to the zero-point spread of the motional wavepacket of the ion. The quantization axis is defined by the magnetic field $\mathbf{B} = B\mathbf{x}$, with \mathbf{x} the unit vector along x . A SDK is generated by two pulse trains $\mathcal{W}(t)$ of duration T_{SDK} composed of pulses $\mathcal{A}(t)$ of duration τ separated by equispaced intervals t_{rep} . (b) Generic energy level diagram (not to scale) of the Raman transition, where the Raman beams have a frequency difference δ that does not necessarily match the qubit splitting ω_{hf} . The higher-frequency beam is detuned from the excited state $|e\rangle$ by Δ .

duration τ is much shorter than the intrinsic qubit dynamics, $2\pi/\tau \gg \omega_{\text{hf}} \gg \omega_t$, so the pulses are approximated by a delta function; and (iii) the SDK protocol time T_{SDK} satisfies $T_{\text{SDK}} \ll 2\pi/\omega_t$, so the ion is effectively frozen during the interaction dynamics and motion can be neglected.

Protocols with a large number of pulses are usually impractical, as they would prolong the SDK time, unlike experiments that employ a limited number of pulses [38, 47, 50]. Moreover, in such experiments the pulse duration is not well separated from the qubit dynamical timescale, so that non-negligible qubit evolution may occur during the pulse interaction, making the instantaneous-pulse assumption not sufficient. In addition, the ion undergoes harmonic motion during the SDK time, which can be comparable to the motional period, and thus deteriorate the performance of the SDK protocol. In the following three sections, we eliminate each one of these approximations individually. However, let us now discuss the results given these simplifications.

Mathematically, the target SDK operator takes the form

$$\hat{U}_{\text{SDK}} = \hat{\mathcal{D}}(i\eta)\hat{\sigma}^+ + \hat{\mathcal{D}}(-i\eta)\hat{\sigma}^-, \quad (2)$$

where $\hat{\mathcal{D}}(\alpha) = \exp\{\alpha\hat{a}^\dagger - \alpha^*\hat{a}\}$ is the displacement operator, $\hat{\sigma}^+$ ($\hat{\sigma}^-$) is the spin raising (lowering) operator, and $\eta = k_d x_0$ is the Lamb-Dicke parameter, with $x_0 = \sqrt{\hbar/(2M\omega_t)}$ corresponding to the zero-point motion spread of the ion with mass M . If the ion is initially in a state $|Q, \alpha\rangle$, where $|\alpha\rangle$ is a coherent state with amplitude $\alpha \in \mathbb{C}$, the ideal target state produced by the operator in Eq. (2) is

$$\hat{U}_{\text{SDK}} |Q, \alpha\rangle = |Q \oplus 1, \alpha + (-1)^Q i\eta\rangle, \quad (3)$$

where \oplus denotes addition modulo 2. In our scheme, the Raman beams consist of trains of short pulses, so the interaction term in Eq. (1) becomes

$$\hat{H}_{\text{int}}(t) = \sum_{n=0}^{N-1} \hat{H}_{\text{pulse}}(t, t_n), \quad (4)$$

with N the number of pulses and the n -th pulse pair term given by

$$\hat{H}_{\text{pulse}}(t, t_n) = \mathcal{A}(t - t_n) \sin(\eta(\hat{a}^\dagger + \hat{a}) + \delta t) \hat{\sigma}_x, \quad (5)$$

where $\mathcal{A}(t)$ is the pulse envelope and t_n is the arrival time of the n -th pulse pair. We have assumed $\varphi_0 = 0$ without loss of generality.

In the limit given by approximation (ii): $\mathcal{A}(t) = \theta\delta(t)$, with pulse amplitude $\theta = \pi/N$, the evolution operator for a single pulse pair arriving at time $t = t_n$, $\hat{U}(t_n)$, has an analytical expression, so its action on a state $|Q, \alpha\rangle$ results in

$$\hat{U}(t_n) |Q, \alpha\rangle = \sum_{m=-\infty}^{\infty} e^{-im\delta t_n} J_m(\theta) \hat{\sigma}_x^m |Q, \alpha - im\eta\rangle, \quad (6)$$

where J_m is the m -th order Bessel function of the first kind. The state in Eq. (6) represents an infinite superposition of displaced coherent states with even/odd spin flips, with rapidly decreasing

amplitudes when the order m increases. The operator $\hat{U}(t_n)$ by itself is not useful for quantum information applications; however, a suitable combination of these idealized pulses approximates the SDK operator in Eq. (2) by meeting the conditions [38, 40]

$$(\delta - \omega_{\text{hf}}) t_n \neq 0 \pmod{2\pi}, \quad (7)$$

$$(\delta + \omega_{\text{hf}}) t_n = 0 \pmod{2\pi}, \quad (8)$$

that become exact in the limit $N \rightarrow \infty$. The pulse pair arrival times need not be equispaced; however, we consider evenly spaced pulses throughout this work, which is easier to implement experimentally by using ad hoc laser sources [52].

3 Optimal few-delta-pulse protocols

In pursuit of faster quantum gates, SDK protocols with a small number of pulses are desirable [38, 47, 50]. Accordingly, in this section we generalize previous SDK theory by removing the infinite-pulse number approximation and instead consider protocols made up of a finite number of delta pulses, while neglecting ion motion, highlighting the differences with the infinite pulse number limit. Under these assumptions, we simplify the description of the model by taking x as a constant of motion and optimize the pulse repetition time t_{rep} and Raman frequency difference δ to best approximate a SDK.

3.1 Formulation

We consider the protocol for creating a SDK described in Sec. 2.2. Since ion motion is neglected, $\hat{H}_t = 0$ in Eq. (1), the position x can be treated as a parameter. Thus, the pulse pair term in Eq. (5) becomes

$$\hat{H}_{\text{pulse}}(t, t_n, \phi_{kx}) = \mathcal{A}(t - t_n) \sin(\phi_{kx} + \delta t) \hat{\sigma}_x, \quad (9)$$

where $\phi_{kx} = k_d x = \eta u$, with $u = x/x_0$ the normalized position. The N delta pulses, $\mathcal{A}(t) = \theta \delta(t)$, have the same area $\theta = \pi/N$ and equispaced arrival times $t_n = n t_{\text{rep}}$, with $n \in \mathbb{N}_0$. The pulse train operator only acts on spin space and is x -dependent. It is obtained by concatenation of a pulse pair operator at time t_n

$$\hat{\mathcal{U}}^{(1)}(t_n, \phi_{kx}) = e^{-i\theta \sin(\phi_{kx} + \delta t_n) \hat{\sigma}_x}, \quad (10)$$

and free evolution operator

$$\hat{\mathcal{U}}_{\text{FE}}^{(\text{hf})}(\mathcal{T}) = e^{-i \frac{\omega_{\text{hf}}}{2} \mathcal{T} \hat{\sigma}_z}, \quad (11)$$

for time $\mathcal{T} = t_{\text{rep}}$ to yield

$$\hat{\mathcal{U}}_N^{(1)}(\phi_\delta, \phi_{\text{hf}}, \phi_{kx}) = \prod_{n=0}^{N-2} \left[e^{-i\theta \sin(\phi_{kx} + (N-n-1)\phi_\delta) \hat{\sigma}_x} e^{-i \frac{\phi_{\text{hf}}}{2} \hat{\sigma}_z} \right] \hat{\mathcal{U}}^{(1)}(t_0, \phi_{kx}), \quad (12)$$

with the angles defined as $\phi_\delta = \delta t_{\text{rep}}$ and $\phi_{\text{hf}} = \omega_{\text{hf}} t_{\text{rep}}$.

The SDK target operator in Eq. (2), with the approximation $\eta(\hat{a}^\dagger + \hat{a}) \approx \phi_{kx}$, is reexpressed as

$$\hat{\mathcal{U}}_{\text{SDK}}(\phi_{kx}, \xi) = e^{i\xi} e^{i\phi_{kx}} \hat{\sigma}^+ + e^{-i\phi_{kx}} \hat{\sigma}^- = \begin{pmatrix} 0 & e^{i\xi} e^{i\phi_{kx}} \\ e^{-i\phi_{kx}} & 0 \end{pmatrix}, \quad (13)$$

where we have introduced ξ as the relative phase between upward (positive, $e^{i\phi_{kx}}$) and downward (negative, $e^{-i\phi_{kx}}$) kick (phase), which we need to incorporate in the target operator so that $\hat{\mathcal{U}}_N^{(1)}$ and $\hat{\mathcal{U}}_{\text{SDK}}$ can be faithfully compared. We use the state-averaged process fidelity as the figure of merit to measure how close the pulse train operator in Eq. (12) is to the SDK operator in Eq. (13)

$$\bar{\mathcal{F}}(\phi_\delta, \phi_{\text{hf}}) = \max_{\xi \in [0, 2\pi)} \frac{1}{2^2} \int_{-\infty}^{\infty} \left| \sum_Q \langle Q | \hat{\mathcal{U}}_{\text{SDK}}^\dagger(u, \xi) \hat{\mathcal{U}}_N^{(1)}(u) | Q \rangle \right|^2 P_{\hat{\rho}}(u) du, \quad (14)$$

where $P_{\hat{\rho}}(u) = \langle u | \hat{\rho} | u \rangle$ is the probability that the ion is at position u assuming it is in a motional state $\hat{\rho} = |\alpha\rangle \langle \alpha|$ (we generalize Eq. (14) by introducing $\hat{\rho}$, as we will also consider thermal states). Equation (14) is interpreted as the process fidelity at every position weighted by the motional wavefunction of the ion. For a more meaningful discussion of the results, in what follows we will use the state-averaged infidelity

$$\bar{\mathcal{I}} = 1 - \bar{\mathcal{F}}. \quad (15)$$

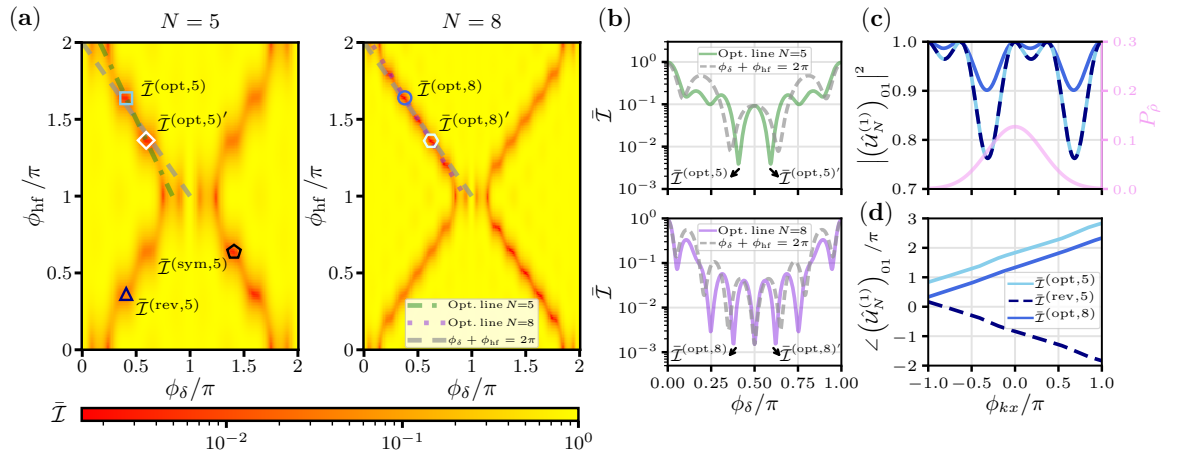


Figure 2. (a) Infidelity landscape comparison between protocols with $N = 5$ (left) and $N = 8$ (right) delta pulses and ion in motional ground state $|f\rangle = |0\rangle$, where the lowest-infidelity points fall in the vicinity of the anti-diagonal line in Eq. (17). $\bar{\mathcal{I}}^{(\text{opt},N)}$ and $\bar{\mathcal{I}}^{(\text{opt},N)'}$ denote the optimal infidelity (that define the optimal line where the local minima are located, which is tilted with respect to the anti-diagonal), $\bar{\mathcal{I}}^{(\text{sym},N)}$ is the corresponding symmetry point, while $\bar{\mathcal{I}}^{(\text{rev},N)}$ denotes the “reverse-kick” optimal infidelity that best approximates $\hat{\mathcal{U}}_{\text{SDK}}(-\phi_{kx})$. (b) Cuts comparing local infidelity minima along the anti-diagonal line in Eq. (17) (dashed), and the optimal lines (solid) exhibiting notably better infidelities. (c) Modulus squared of the off-diagonal element (left axis) $|\hat{\mathcal{U}}_N^{(1)}|_{01}^2$ versus ϕ_{kx} for the optimal infidelities $\bar{\mathcal{I}}^{(\text{opt},N)}$ and $\bar{\mathcal{I}}^{(\text{rev},N)}$. The right axis represents the position probability distribution of the ground state of motion $|f\rangle = |0\rangle$. (d) Phase of the element $\angle(\hat{\mathcal{U}}_N^{(1)})_{01}$ versus ϕ_{kx} for $\bar{\mathcal{I}}^{(\text{opt},N)}$ and $\bar{\mathcal{I}}^{(\text{rev},N)}$.

3.2 Methodology

We want to find the point(s) that show the smallest infidelity for different number of pulses with the ion in a certain motion state. The search space consists of points $\{\{\phi_\delta, \phi_{\text{hf}}\} : \phi_\delta, \phi_{\text{hf}} \in [0, 2\pi)\}$, which can be represented in a 2D map, as in Fig. 2(a). The infidelity landscape presents some symmetry, a point $\{\phi_\delta, \phi_{\text{hf}}\}$ in the left half of the map has a corresponding point in the right half $\{\phi_\delta + \pi, \phi_{\text{hf}} - \pi \pmod{2\pi}\}$ with the same infidelity value, simplifying the search for $\phi_\delta \in [0, \pi)$ and $\phi_{\text{hf}} \in [0, 2\pi)$.

We find that the lower-infidelity points concentrate in bands that lie in the environment of

$$\phi_\delta - \phi_{\text{hf}} = 0, \quad (16)$$

which corresponds to Eq. (7) with equality sign (it simplifies to $\delta = \omega_{\text{hf}}$, the continuous-wave resonant condition), and

$$\phi_\delta + \phi_{\text{hf}} = 2\pi, \quad (17)$$

corresponding to Eq. (8).

We perform an optimization of the infidelity in Eq. (15) for protocols of different number of pulses assuming that the ion is in a given Gaussian motional state, either a coherent state or a thermal state with average number of phonons $\bar{n} = 1/(\exp\{\hbar\omega_t/(k_B T)\} - 1)$, where k_B is the Boltzmann’s constant and T is the temperature. Our optimization strategy uses multiple initial seeds and identifies the optimal solution as the converged solution with the lowest infidelity. Due to symmetry, the seeds are placed in the left half of the map. They include the local infidelity minima along the anti-diagonal line in Eq. (17) (see Fig. 2(b)) and the global maxima along the lines $\phi_{\text{hf}} = \pi$ and $\phi_{\text{hf}} = 2\pi$; see Fig. 2(a). We do not incorporate as initial seeds the local maxima along the diagonal line in Eq. (16), as they match the forbidden condition outlined in Eq. (7) and, as will be justified later, correspond to points that approximate the “reverse-kick” SDK operator $\hat{\mathcal{U}}_{\text{SDK}}(-\phi_{kx})$.

For the discussion of the results we will also refer to two characteristics concerning the off-diagonal element of the pulse train operator in Eq. (12), $(\hat{\mathcal{U}}_N^{(1)})_{01}$, as compared to the corresponding element of the ideal SDK unitary operator in Eq. (13): (i) the squared modulus $|\hat{\mathcal{U}}_N^{(1)}|_{01}|^2$, which ideally should be equal to 1, and (ii) the relationship of the phase $\angle(\hat{\mathcal{U}}_N^{(1)})_{01}$ with ϕ_{kx} , which is linear in the ideal case.

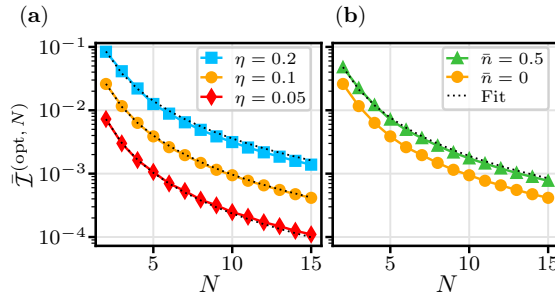


Figure 3. Delta-pulse optimal state-averaged infidelity versus pulse number in the protocol. (a) Results for ion in motional ground state $|f\rangle = |0\rangle$ for different values of the Lamb–Dicke parameter. The fit parameters $\{K, r\}$ of the power-law decay $\bar{\mathcal{I}}^{(\text{opt}, N)} = KN^{-r}$ (dotted lines) are $\{0.33, 1.96\}$, $\{0.11, 2.05\}$ and $\{0.03, 2.13\}$ for $\eta = 0.2, 0.1, 0.05$, respectively. (b) Comparison of the optimal infidelity for the ground state ($\bar{n} = 0$) and a thermal state with $\bar{n} = 0.5$, both for $\eta = 0.1$. The fit parameters for $\bar{n} = 0.5$ are $\{0.19, 2.00\}$.

3.3 Results

Following the optimization strategy described, we find two optimal solutions, $\{\phi_\delta^{(\text{opt}, N)}, \phi_{\text{hf}}^{(\text{opt}, N)}\}$ and $\{\phi_\delta^{(\text{opt}, N)'}, \phi_{\text{hf}}^{(\text{opt}, N)'}\}$, that present the same infidelity value $\bar{\mathcal{I}}^{(\text{opt}, N)}$, related by:

$$\left\{ \phi_\delta^{(\text{opt}, N)'}, \phi_{\text{hf}}^{(\text{opt}, N)'} \right\} = \left\{ \pi - \phi_\delta^{(\text{opt}, N)}, \pi - \phi_{\text{hf}}^{(\text{opt}, N)} \pmod{2\pi} \right\}, \quad (18)$$

and two additional points in the right half of the map that follow from the symmetry relation described:

$$\left\{ \phi_\delta^{(\text{sym}, N)}, \phi_{\text{hf}}^{(\text{sym}, N)} \right\} = \left\{ \phi_\delta^{(\text{opt}, N)} + \pi, \phi_{\text{hf}}^{(\text{opt}, N)} - \pi \pmod{2\pi} \right\}. \quad (19)$$

For a small number of pulses, the “optimal line” containing the local minima is tilted with respect to the ideal $N \rightarrow \infty$ condition in Eq. (17)—the anti-diagonal line—and presents visibly better infidelity values; see Fig. 2(a-b). Furthermore, we show that there are a limited number of good-infidelity points, contrary to the full span of the anti-diagonal. As the number of pulses increases, the low-infidelity bands become narrower, develop more numerous and deeper local minima, and align more closely with Eqs. (16) and (17). This behavior is consistent with Refs. [38, 40], which predict vanishing infidelity in the anti-diagonal region in the limit of an infinite number of pulses.

We find that the optimal infidelity $\bar{\mathcal{I}}^{(\text{opt}, N)}$ follows a power-law decay with increasing pulse number: $\bar{\mathcal{I}}^{(\text{opt}, N)} = KN^{-r}$, with $K, r \in \mathbb{R}$, as shown in Fig. 3. $\bar{\mathcal{I}}^{(\text{opt}, N)}$ becomes greater with increasing width of the ionic motional wavepacket, caused either by a larger Lamb–Dicke parameter or higher temperature. This is due to the SDK protocol not having the same quality at every position throughout the trap. Therefore, the state-averaged infidelity will be smaller if the ion is more localized in positions where the overlap $\langle Q | \hat{U}_{\text{SDK}}^\dagger \hat{U}_N^{(1)} | Q \rangle$ is maximal.

This position dependence is manifested in the value $|\hat{U}_N^{(1)}|_{01}^2$ for the optimal infidelities $\bar{\mathcal{I}}^{(\text{opt}, N)}$. It presents a maximum coinciding with the ideal one at the position where it is most likely to find the ion, and a decrease for farther values of x ; see Fig. 2(c). The higher optimal infidelity seen for the protocol with fewer pulses is evidenced by the greater deviation of $|\hat{U}_N^{(1)}|_{01}^2$ from 1 as we move away from $x = 0$.

The phase of $(\hat{U}_N^{(1)})_{01}$ shows an approximate linear relationship with ϕ_{kx} , as depicted in Fig. 2(d). A root-mean-square measure of this linearity reveals a better adjustment for the protocol with a higher pulse number. The y-intercept unveils the value of ξ in the definition of \hat{U}_{SDK} in Eq. (13). Points lying around the diagonal line in Eq. (16) show a reverted kick direction, as evidenced by the negative slope. The pair $\{\phi_\delta^{(\text{rev}, N)}, \phi_{\text{hf}}^{(\text{rev}, N)}\}$, with $\phi_\delta^{(\text{rev}, N)} = \phi_\delta^{(\text{opt}, N)}$ and $\phi_{\text{hf}}^{(\text{rev}, N)} = 2\pi - \phi_{\text{hf}}^{(\text{opt}, N)}$, constitutes the optimal point if we target $\hat{U}_{\text{SDK}}(-\phi_{kx})$, which corresponds to a SDK operator with the kick direction exchanged for each spin state. This explains the local infidelity maximum at $\{\pi, \pi\}$, consistent with Eqs. (7) and (8), which must not be fulfilled simultaneously. The infinite-pulse number exact conditions for having $\hat{U}_{\text{SDK}}(-\phi_{kx})$ result from swapping the “ \neq ” and “ $=$ ” signs in Eqs. (7) and (8), respectively [38, 40].

For a given atomic isotope of mass M excited by light with wavenumber k the Lamb–Dicke parameter η can be reduced by increasing the trap frequency. η is an important parameter, since faster two-qubit gate schemes that rely on sequences of SDKs require either more SDKs or smaller

trap frequencies [47]. In addition, there exists a trade-off between kick strength ηu (required for enough geometric phase accumulation in two-qubit gate schemes [40]) and fidelity.

These results illustrate how the semiclassical approach provides more insight into the dependence of infidelity on the Lamb–Dicke parameter and temperature.

4 Finite-width pulse protocols

We now consider finite pulse train protocols with pulses of finite width in the absence of ion motion, to quantify the impact of neglecting the pulse temporal profile on the infidelity.

Trapped-ion hyperfine qubits have typical frequencies $\omega_{\text{hf}} \sim 1\text{--}20$ GHz [53] so, if excited by a mode-locked picosecond laser source (with pulse duration in the range $\tau \sim 1\text{--}20$ ps), the hyperfine period and the pulse duration timescales are not well separated, and this will prove to be the dominant source of error. This differs from the ideal dynamics of the few instantaneous pulses considered in the previous section.

4.1 Formulation

We still neglect the trap potential term and now lift the instantaneous-pulse approximation, so we consider the pulse pair Hamiltonian in Eq. (9) with the more realistic pulse envelope modeled as a Gaussian profile

$$\mathcal{A}(t) = \frac{\theta}{\sqrt{2\pi\sigma^2}} e^{-\frac{t^2}{2\sigma^2}}, \quad (20)$$

where σ^2 is the variance, and the pulse width $\tau = \sigma\sqrt{8\log 2}$ is taken as the full-width at half-maximum of the Gaussian.

The temporal dependence of the pulse envelope in Eq. (20) does not allow for a closed-form analytical solution of the evolution operator for a single finite-width pulse pair, as was the case for delta pulses. Therefore, we approximate the propagator numerically using Trotterization. For the considered extension of the pulse $t_{\text{ext}} = m\sigma$, where m is the number of standard deviations spanning the truncated Gaussian, the pulse pair operator is computed as

$$\hat{\mathcal{U}}^{(2)}(t, t_n, \phi_{kx}) = \prod_{s=0}^{S-1} \exp \left\{ -i \left[\hat{H}_{\text{hf}} + \hat{H}_{\text{pulse}}(t_s + dt/2, t_n, \phi_{kx}) \right] dt \right\}, \quad (21)$$

where $t_s = t_n - t_{\text{ext}}/2 + sdt$, S is the number of Trotter steps and $dt = t_{\text{ext}}/S$ is the differential time step. The pulse train operator thus reads

$$\hat{\mathcal{U}}_N^{(2)}(t, \phi_{kx}) = \prod_{n=0}^{N-2} \left[\hat{\mathcal{U}}^{(2)}(t, t_n, \phi_{kx}) \hat{\mathcal{U}}_{\text{FE}}^{(\text{hf})}(t_{\text{rep}} - t_{\text{ext}}) \right] \hat{\mathcal{U}}^{(2)}(t, t_0, \phi_{kx}). \quad (22)$$

We take the same expression for the target SDK operator given in Eq. (13) and the fidelity in Eq. (14) with the corresponding operator $\hat{\mathcal{U}}_N^{(2)}$.

4.2 Methodology

At the level of a single pulse pair, the non-commuting qubit (\hat{H}_{hf}) and pulse pair ($\hat{H}_{\text{pulse}}(t, t_n, \phi_{kx})$) terms introduce an error in the interaction dynamics relative to the ideal delta-pulse scenario. We use time-dependent perturbation theory to compute an error bound due to the finite duration of each pulse, where the slow \hat{H}_{hf} term in Eq. (1) is treated perturbatively with respect to $\hat{H}_{\text{pulse}}(t, t_n, \phi_{kx})$. To this end, we express the pulse pair evolution operator as

$$\tilde{\mathcal{U}}^{(2)}(t, t_n, \phi_{kx}) = \hat{\mathcal{U}}_{\text{pulse}}(t, t_n, \phi_{kx}) \hat{\mathcal{U}}_{\text{hf}}(t, t_n, \phi_{kx}), \quad (23)$$

where

$$\hat{\mathcal{U}}_{\text{pulse}}(t, t_n, \phi_{kx}) = \exp \left\{ -i \int_{t_n - t_{\text{ext}}/2}^t \hat{H}_{\text{pulse}}(t', t_n, \phi_{kx}) dt' \right\}, \quad (24)$$

$$\frac{d}{dt} \hat{\mathcal{U}}_{\text{hf}}(t, t_n, \phi_{kx}) = -i \hat{H}_{\text{hf}}^{(1)}(t, t_n, \phi_{kx}) \hat{\mathcal{U}}_{\text{hf}}(t, t_n, \phi_{kx}), \quad (25)$$

$$\hat{H}_{\text{hf}}^{(1)}(t, t_n, \phi_{kx}) = \hat{\mathcal{U}}_{\text{pulse}}^\dagger(t, t_n, \phi_{kx}) \hat{H}_{\text{hf}} \hat{\mathcal{U}}_{\text{pulse}}(t, t_n, \phi_{kx}). \quad (26)$$

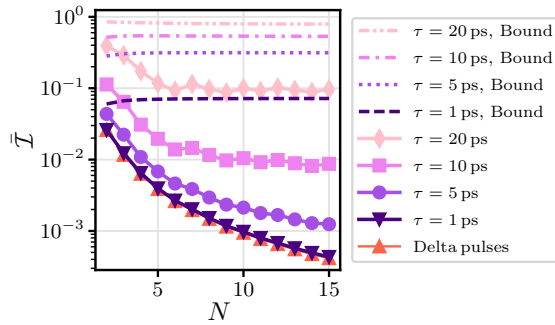


Figure 4. Infidelity versus pulse number evaluated at $\{\phi_{\delta}^{(\text{opt},N)}, \phi_{\text{hf}}^{(\text{opt},N)}\}$ for different pulse widths (the points $\{\phi_{\delta}^{(\text{opt},N)'}, \phi_{\text{hf}}^{(\text{opt},N)'}\}$ exhibit larger deterioration, not shown) and error bound $N\tilde{\epsilon}_{\Omega}$. We have considered a $^{133}\text{Ba}^+$ ion ($\omega_{\text{hf}} \approx 2\pi \times 10 \text{ GHz}$) in the ground state of motion $|f\rangle = |0\rangle$ with $\eta = 0.1$.

If $\hat{H}_{\text{pulse}}(t, t_n, \phi_{kx})$ and \hat{H}_{hf} commuted, we would have $\hat{U}_{\text{hf}}(t, t_n) = \hat{U}_{\text{FE}}^{(\text{hf})}(t - (t_n - t_{\text{ext}}/2))$; however, that is not the case, so we approximate $\hat{U}_{\text{hf}}(t, t_n, \phi_{kx}) \approx \tilde{\mathcal{U}}_{\text{hf}}(t, t_n)$ using the Magnus expansion. The single-pulse pair error is thus defined as

$$\tilde{\epsilon}_{\Omega} = \left\| \hat{U}_{\text{FE}}^{(\text{hf})}(\tau) - \tilde{\mathcal{U}}_{\text{hf}}(t_n + \tau/2, t_n) \right\|, \quad (27)$$

where $\|\cdot\|$ denotes matrix norm. It can be approximated as (see Appendix A)

$$\tilde{\epsilon}_{\Omega}(\tau, N) \approx \frac{\omega_{\text{hf}}\tau}{2} \sqrt{1 - \text{sinc}\left(\frac{\gamma}{N}\right) \left[2 \cos\left(\frac{\beta}{N}\right) - \text{sinc}\left(\frac{\gamma}{N}\right) \right]}, \quad (28)$$

where $\beta = \pi \text{erf}(-\sqrt{\log 2})$, $\gamma = 2\sqrt{\pi \log 2}$, and $\text{sinc}(a) = \sin(a)/a$. The error propagates for each pulse pair, so the total error bound is

$$1 - [1 - \tilde{\epsilon}_{\Omega}(\tau, N)]^N \approx 1 - [1 - N\tilde{\epsilon}_{\Omega}(\tau, N)] = N\tilde{\epsilon}_{\Omega}(\tau, N), \quad (29)$$

where we have approximated $[1 - \tilde{\epsilon}_{\Omega}(\tau, N)]^N$ to first order in $\tilde{\epsilon}_{\Omega}(\tau, N)$. The dependence with the number of pulses for large N vanishes to leading order

$$N\tilde{\epsilon}_{\Omega}(\tau, N) \approx \frac{\omega_{\text{hf}}\tau}{2} |\beta| + \mathcal{O}(N^{-2}). \quad (30)$$

We compare this error bound with numerical simulations of the pulse train operator in Eq. (22) evaluated at the delta-pulse optimal points.

4.3 Results

We simulate the protocol with finite-width pulses introducing the ion species $^{133}\text{Ba}^+$ ($\omega_{\text{hf}} \approx 2\pi \times 10 \text{ GHz}$) without loss of generality.

We observe that the infidelity of the protocol with pulses of finite width is degraded with increasing pulse duration with respect to the value obtained for delta pulses, except for very short pulses $\tau \sim 1\text{--}5 \text{ ps}$; see Fig. 4. In this case, the product of the hyperfine frequency and the pulse width yields $\tau\omega_{\text{hf}}/(2\pi) = 1\text{--}5 \times 10^{-2}$, which serves as an indicator to evaluate the validity of the delta-pulse approximation. This is a consequence of the different orientations in Pauli space of \hat{H}_{hf} and $\hat{H}_{\text{pulse}}(t, t_n, \phi_{kx})$, which cause the pulse pair to generate a rotation of the qubit about an axis distinct from the pure $\hat{\sigma}_x$ -rotation present in the delta-pulse limit. This demonstrates that the optimal points found assuming instantaneous pulses are not necessarily optimal for finite-width pulse protocols and are thus displaced.

The single-pulse pair error accumulates as more pulses are added so, for a given pulse width, the error relative to the delta-pulse infidelity increases with pulse number. We find a 100% relative error for protocols with 7–9 pulses and pulse duration as low as 5 ps. The infidelity suffers an order of magnitude rise (with respect to the delta-pulse value) with 10 pulses 10 ps-long, whereas it becomes two orders of magnitude greater with 20 ps pulses. Even though the analytic bound is pessimistic, it correctly predicts the infidelity saturation observed for sufficiently large pulse number. In contrast to the delta-pulse case, where the infidelity continues to improve with increasing pulse number, there is no such improvement for higher-width pulses, as the gain is counteracted by the pulse width error.

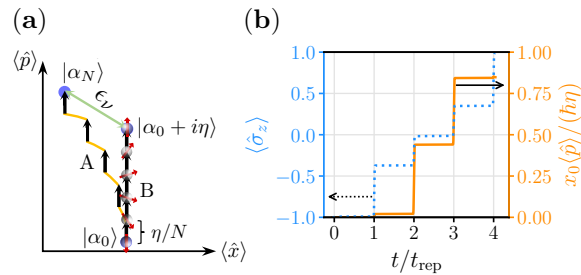


Figure 5. (a) Phase space picture of a 5-pulse SDK with (path A) and without (path B) taking into account the secular motion of the ion, assuming equal-strength momentum kicks $p = \eta/N$ (in units of \hbar/x_0) depicted as black arrows. The error ϵ_ν is regarded as the distance between the final states $|\alpha_N\rangle$ and $|\alpha_0 + i\eta\rangle$. The red arrows represent the spin state, which rotates with every momentum displacement (only shown in path B for visibility). (b) SDK simulation including ion motion for $N = 5$ pulses of duration 5 ps at the delta-pulse optimal point with $t_{\text{rep}} \approx 0.28$ ns in a trap of frequency $\omega_t = 2\pi \times 2$ MHz. The expectation values $\langle \hat{\sigma}_z \rangle$ (left axis, dotted) and $\langle \hat{p} \rangle$ (right axis, solid) are depicted throughout the SDK time. In contrast to the simple process illustrated in panel (a), the momentum kick provided by each pulse has a different value; in this particular case, only the third and fourth pulses mainly contribute to the momentum transfer.

5 Ion motion

Having considered in the previous section the real characteristics of picosecond pulses, we now lift the zero-motion approximation and we simulate the complete model. In the timescale of the SDK time around a few nanoseconds long, ion motion is expected to be small for typical trap frequencies in the megahertz range; nonetheless we characterize the influence of ion secular motion on the infidelity, both analytically and numerically, finding a negligible error compared with that due to the finite pulse duration.

5.1 Formulation

For convenience, we restate the complete Hamiltonian in Eq. (1) ($\varphi_0 = 0$)

$$\hat{H} = \omega_t \hat{a}^\dagger \hat{a} + \frac{\omega_{\text{hf}}}{2} \hat{\sigma}_z + \mathcal{W}(t) \sin(\eta(\hat{a}^\dagger + \hat{a}) + \delta t) \hat{\sigma}_x. \quad (31)$$

The ion is allowed to move in a harmonic oscillator potential and the pulse interaction term, given in Eq. (5), has the position as a quantum operator.

In this section, we assume that the ion is initially in a spin-coherent state $|Q, \alpha_0\rangle$, so the final evolved state is given by $\hat{U}_N^{(3)} |Q, \alpha_0\rangle$ (details on the state propagation given in Appendix B). The infidelity in the combined spin-motion Hilbert space is defined as

$$\mathcal{I} = 1 - \left| \langle Q, \alpha_0 | \hat{U}_{\text{SDK}}^\dagger \hat{U}_N^{(3)} | Q, \alpha_0 \rangle \right|^2. \quad (32)$$

5.2 Methodology

The trap potential (\hat{H}_t) and pulse pair ($\hat{H}_{\text{pulse}}(t, t_n)$) hamiltonians do not commute; however, we have $\tau \int \mathcal{A}(t - t_n) dt \gg \omega_t \tau$ by 5–6 orders of magnitude. Therefore, for the theoretical error estimation we assume the delta-pulse scenario, in which the ion gets N instantaneous momentum kicks separated with harmonic free evolution for a time t_{rep} . The error is thus measured as

$$\tilde{\epsilon}_\nu = 1 - |\langle \alpha_0 + i\eta | \alpha_N \rangle|^2, \quad (33)$$

where α_0 is the amplitude of the initial coherent state and $|\alpha_N\rangle$ is the idealized final coherent state after N kicks of momentum $p = \eta/N$ (in units of \hbar/x_0) with motion between pulses; see Fig. 5(a). The state $|\alpha_0 + i\eta\rangle$ corresponds to the target motional state as outlined in Eq. (3). The trap potential term \hat{H}_t does not affect the spin state, so in Eq. (33) we considered the same final spin state for the evolved states with and without motion. Equation (33) can be approximated to (see Appendix C)

$$\tilde{\epsilon}_\nu \approx \left(\frac{\eta \omega_t t_{\text{rep}} (N - 1)}{2} \right)^2. \quad (34)$$

The actual infidelity error caused by the motion is measured as

$$\epsilon_\nu = \mathcal{I}^{(\nu)} - \mathcal{I}^{(\Omega)}, \quad (35)$$

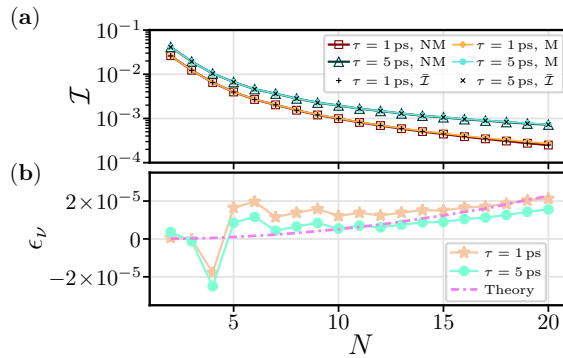


Figure 6. SDK simulation for the ion initially in the state $|\Psi_0\rangle = |1\rangle|0\rangle$ with $(M, \mathcal{I}^{(\nu)})$ and without $(NM, \mathcal{I}^{(\Omega)})$ ion motion at the delta-pulse optimal points for different pulse durations. The parameter values are $t_{\text{rep}} \approx 0.25\text{--}0.28$ ns, $\omega_{\text{hf}} \approx 2\pi \times 10$ GHz and $\omega_t = 2\pi \times 2$ MHz. (a) Infidelity versus pulse number compared to the semiclassical values $\tilde{\mathcal{I}}$, where position is treated as a parameter. (b) Difference between infidelities with and without ion motion, and theoretical error estimation $\tilde{\epsilon}_\nu$ in Eq. (34).

where $\mathcal{I}^{(\nu)}$ and $\mathcal{I}^{(\Omega)}$ are the infidelities with and without ion motion, respectively, at the delta-pulse optimal points.

Contrary to the theoretical error calculation where we assumed instantaneous pulses, we perform simulations considering finite-duration pulses with and without the trap potential term \hat{H}_t . We extract the repetition time t_{rep} and the Raman frequency difference δ from the delta-pulse optimal points and evaluate the infidelity in Eq. (32).

5.3 Results

In our simulations we consider a $^{133}\text{Ba}^+$ ion ($\omega_{\text{hf}} \approx 2\pi \times 10$ GHz) in a $\omega_t = 2\pi \times 2$ MHz trap excited by light with center wavelength $\lambda = 532$ nm (each beam is shifted in frequency by $\pm\delta/2$), so that the Lamb–Dicke parameter is $\eta \approx 0.1$.

For t_{rep} of fractions of ns (so that $T_{\text{SDK}} \sim \text{ns}$, as in Refs. [38, 50, 47]) we obtain minimal deterioration of the infidelity when the motion of the ion is included; see Fig. 6. The error is of the order of 10^{-5} for $T_{\text{SDK}}\omega_t/(2\pi) = 5\text{--}5.6 \times 10^{-4}N$, orders of magnitude smaller than the dominating error due to the finite pulse duration. This is due to the ion falling in trap zones where the protocol deviates from the ideal operation. Moreover, we find excellent agreement with the semiclassical infidelity defined in Eq. (15), which proves to be an accurate description when the motion of the ion does not play a role in the dynamics.

We identify two regions with different error trends in Fig. 6(b). For $N \gtrsim 7$ we see a clear increasing tendency as more pulses are added to the realization of the SDK—since the larger the protocol time T_{SDK} the more the ion moves—which is closely followed by the analytical error in Eq. (34). This matching is more apparent for $\tau = 1$ ps, as the pulses behave effectively as delta pulses for the considered $\omega_{\text{hf}} \approx 2\pi \times 10$ GHz. We observe a smaller error ϵ_ν for broader pulses, which is corroborated numerically due to a smaller ion displacement. For $N \lesssim 7$ the error does not have a predictable behavior, although it remains within the same order of magnitude anticipated by the theoretical error in Eq. (34). Due to the temporal dependence of the sine term in the Rabi frequency (see Eq. (31)), the momentum provided by each pulse is different, as represented in Fig. 5(b), and is more evenly distributed among pulses for protocols with larger N , which differs from the simple scheme depicted in Fig. 5(a). As a consequence, the motion of the ion is almost always larger than the theoretical prediction (it has the opposite behavior for $|\Psi_0\rangle = |0\rangle|0\rangle$, not represented).

6 Conclusions and outlook

We accurately find the optimal points $\{\phi_\delta, \phi_{\text{hf}}\}$ (related to the frequency difference between the Raman beams, the repetition time between the pulses and the hyperfine qubit frequency) by optimizing SDK infidelity on a stationary ion with the exact, few-delta-pulse propagator (with equispaced, equal-amplitude pulses), which differ from the large pulse number limit conditions [38, 40].

The optimal infidelity follows a power-law decay with the number of pulses, which rapidly goes below 10^{-3} for ~ 10 pulses (with $\eta = 0.1$ and the ion in the ground state of motion). We find that the optimal infidelity increases as the motional wavepacket of the ion becomes wider either by a

larger Lamb–Dicke parameter or higher temperature, which displaces the optimal points, and is easily inferred by our semiclassical approach.

We show that SDK infidelity in few-pulse protocols is dominated by finite-pulse duration and not ion motion. The instantaneous-pulse approximation taken in the optimization is only reliable for very short pulses, when $\tau\omega_{\text{hf}}/(2\pi) \sim 1\text{--}5 \times 10^{-2}$, which translates to pulse durations $\tau \sim 1\text{--}5$ ps for hyperfine frequencies $\omega_{\text{hf}} \approx 2\pi \times 10$ GHz. The infidelity error relative to the ideal delta-pulse case deteriorates by one (two) orders of magnitude for 10 pulses of duration 10 ps (20 ps), corresponding to conditions similar to performed experiments [38, 50]. We confirm that ion secular motion introduces a small error of the order of 10^{-5} for typical SDK times $T_{\text{SDK}} \sim \text{ns}$ where the trap frequency is $\omega_t \sim \text{MHz}$ ($T_{\text{SDK}}\omega_t/(2\pi) = 5\text{--}5.6 \times 10^{-4}N$).

Future work could explore ways to increase the fidelity of SDKs. The infidelity deterioration due to the finite pulse duration can be approximately compensated by an increase in the pulse area at the expense of higher laser power [40]. As an improved alternative, due to the critical impact of pulse width, a new optimization of the parameters $\{\phi_\delta, \phi_{\text{hf}}\}$ could be performed accounting for the finite pulse duration. Furthermore, higher fidelities may be achieved if the optimization space is enlarged by having unequal pulse amplitudes and/or arrival times [54, 55], limited by the error bound due to the ion motion that we find here.

This work establishes the relevant aspects to consider when optimizing SDKs with short pulses and provides both theoretical error scalings and actual simulated values of infidelity due to the instantaneous-pulse and frozen-ion approximations. These results determines the optimal working conditions, establishing the path towards the generation of fast two-qubit entangling gates with pulsed sources.

Supplementary data

A Finite-width pulse error estimation

We want to approximate $\hat{U}_{\text{hf}}(t, t_n, \phi_{kx})$ in Eq. (25) using the Magnus expansion to first order

$$\tilde{U}_{\text{hf}}(t, t_n, \phi_{kx}) = e^{\Omega_1(t, t_n, \phi_{kx})}, \quad (36)$$

where

$$\Omega_1(t, t_n, \phi_{kx}) = -i \int_{t_n - \tau/2}^t \hat{H}_{\text{hf}}^{(1)}(t'', t_n, \phi_{kx}) dt''. \quad (37)$$

The Hamiltonian \hat{H}_{hf} in the interaction picture with respect to $\hat{H}_{\text{pulse}}(t'', t_n, \phi_{kx})$ can be expressed as

$$\begin{aligned} \hat{H}_{\text{hf}}^{(1)}(t, t_n, \phi_{kx}) &= e^{i\zeta(t, t_n, \phi_{kx})\hat{\sigma}_x} \hat{H}_{\text{hf}} e^{-i\zeta(t, t_n, \phi_{kx})\hat{\sigma}_x} \\ &= \frac{\omega_{\text{hf}}}{2} (\cos[2\zeta(t, t_n, \phi_{kx})] \hat{\sigma}_z + \sin[2\zeta(t, t_n, \phi_{kx})] \hat{\sigma}_y), \end{aligned} \quad (38)$$

where

$$\zeta(t, t_n, \phi_{kx}) = \int_{t_n - \tau/2}^t \hat{H}_{\text{pulse}}(t', t_n, \phi_{kx}) dt'. \quad (39)$$

A sufficient condition for convergence of the series is

$$\pi > \int_{t_n - \tau/2}^{t_n + \tau/2} \left\| \hat{H}_{\text{hf}}^{(1)}(t, t_n, \phi_{kx}) \right\| = \frac{\omega_{\text{hf}}}{2} \int_{t_n - \tau/2}^{t_n + \tau/2} dt_1 = \frac{\omega_{\text{hf}}\tau}{2}, \quad (40)$$

which is fulfilled for $\tau \lesssim 100$ ps if $\omega_{\text{hf}} \approx 2\pi \times 10$ GHz. To compute the matrix norm we used $\|A\| = |c_1| + \sqrt{|c_x|^2 + |c_y|^2 + |c_z|^2}$, for any 2×2 real matrix $A = c_1\mathbb{I} + c_x\sigma_x + c_y\sigma_y + c_z\sigma_z$ in the basis $\{\mathbb{I}, \sigma_x, \sigma_y, \sigma_z\}$. Considering the Gaussian pulse envelope in Eq. (20) we have

$$\begin{aligned} \zeta(t, t_n) &\approx \frac{\theta \sin(\phi_{kx} + \delta t_n)}{\sigma\sqrt{2\pi}} \int_{t_n - \tau/2}^t \exp\left\{-\frac{(t' - t_n)^2}{2\sigma^2}\right\} dt' \\ &\approx \frac{\theta'}{2} \left[\frac{1}{\sigma} \sqrt{\frac{2}{\pi}} (t - t_n) - \frac{\beta}{\pi} \right] \leq \frac{\theta}{2} \left[\frac{1}{\sigma} \sqrt{\frac{2}{\pi}} (t - t_n) - \frac{\beta}{\pi} \right]. \end{aligned} \quad (41)$$

In the first line of Eq. (41), we assumed $t - (t_n - \tau/2) \ll 2\pi/\delta$, so that the sine term can be treated as a constant. In the second line, we first Taylor-expanded $\text{erf}[(t - t_n)/(\sigma\sqrt{2})]$ to first order about

$t = t_n$, and we then bounded $\theta' = \theta \sin(\phi_{kx} + \delta t_n) \leq \theta$ (thereby removing the cumbersome dependence on ϕ_{kx}). Therefore, we can compute the first order term in Eq. (37) as

$$\Omega_1(\tau, N) = -i \frac{\omega_{\text{hf}} \tau}{2} \text{sinc}\left(\frac{\gamma}{N}\right) \left[\cos\left(\frac{\beta}{N}\right) \hat{\sigma}_z - \sin\left(\frac{\beta}{N}\right) \hat{\sigma}_y \right]. \quad (42)$$

Using the identity $e^{-i\mathbf{R}\cdot\boldsymbol{\sigma}} = \cos(R)\mathbb{I} - i \sin(R)\mathbf{R}\cdot\boldsymbol{\sigma}/R$, where $\mathbf{R} = (R_x, R_y, R_z)$, $\boldsymbol{\sigma}$ is the vector of Pauli matrices and $R = |\mathbf{R}|$, we expand the operators in Eq. (27) to first order in $\omega_{\text{hf}}\tau$. Then, we compute the matrix norm to arrive to Eq. (28).

B Complete model state propagation

Instead of finding the approximate pulse train operator $\hat{U}_N^{(3)}$, we propagate the state using Trotterization for numerical stability. For the extension of the pulses considered $t \in [t_n - t_{\text{ext}}/2, t_n + t_{\text{ext}}/2]$, the state at each time step during the n -th pulse pair is

$$|\Psi\rangle_{t_{s+1}}^{(t_n)} = \exp\left\{-i \left[\hat{H}_t + \hat{H}_{\text{hf}} + \hat{H}_{\text{pulse}}(t_s + dt/2, t_n, \phi_{kx}) \right] dt\right\} |\Psi\rangle_{t_s}^{(t_n)}, \quad (43)$$

where $t_s = t_n - t_{\text{ext}}/2 + sdt$, with $s = 0, \dots, S$, and $|\Psi\rangle_{t_0 - t_{\text{ext}}/2}^{(t_0)} = |Q\rangle |\alpha_0\rangle$. The wavefunction at the end of the pulse dynamics is therefore $|\Psi\rangle_{t_n + t_{\text{ext}}/2}^{(t_n)}$. Next, we concatenate both qubit and trap free evolution operators for time $\mathcal{T} = t_{\text{rep}} - t_{\text{ext}}$ before the beginning of the next pulse at $t_s = t_{n+1} - t_{\text{ext}}/2$ as

$$|\Psi\rangle_{t_{n+1} - t_{\text{ext}}/2}^{(t_{n+1})} = \hat{U}_{\text{FE}}^{(\text{hf})}(t_{\text{rep}} - t_{\text{ext}}) \hat{U}_{\text{FE}}^{(t)}(t_{\text{rep}} - t_{\text{ext}}) |\Psi\rangle_{t_n + t_{\text{ext}}/2}^{(t_n)}, \quad (44)$$

where we define

$$\hat{U}_{\text{FE}}^{(t)}(\mathcal{T}) = e^{-i\omega_t \mathcal{T} \hat{a}^\dagger \hat{a}}. \quad (45)$$

C Ion motion error estimation

To estimate the error in the design of a SDK when the motion of the ion is considered in the evolution, we assume an ideal delta-pulse train which produces a perfect spin flip and every pulse kicks the ion with momentum $p = \eta/N$, so the exact evolution operator $\hat{U}_N^{(3)}$ can be approximated by

$$\tilde{\hat{U}}_N^{(3)} = \hat{\sigma}_x \otimes \left(\prod_{n=0}^{N-2} \left[\hat{\mathcal{D}}(ip) \hat{U}_{\text{FE}}^{(t)}(t_{\text{rep}}) \right] \hat{\mathcal{D}}(ip) \right). \quad (46)$$

Using

$$\hat{\mathcal{D}}(ip) |\alpha\rangle = |\alpha + ip\rangle, \quad (47)$$

$$\hat{U}_{\text{FE}}^{(t)}(t_{\text{rep}}) |\alpha\rangle = e^{-i\omega_t t_{\text{rep}}/2} |\alpha e^{-i\omega_t t_{\text{rep}}}\rangle, \quad (48)$$

we find recursively $\tilde{\hat{U}}_N^{(3)} |Q\rangle |\alpha_0\rangle = e^{-iN\omega_t t_{\text{rep}}/2} |Q \oplus 1\rangle |\alpha_N\rangle$, with

$$\begin{aligned} \alpha_N &= \alpha_0 e^{-iN\omega_t t_{\text{rep}}} + ip \sum_{n=0}^{N-1} e^{-i\omega_t t_n} \\ &= \alpha_0 e^{-iN\omega_t t_{\text{rep}}} + i \frac{\eta}{N} e^{-i\omega_t t_{\text{rep}}(N-1)/2} \frac{\sin(N\omega_t t_{\text{rep}}/2)}{\sin(\omega_t t_{\text{rep}}/2)}. \end{aligned} \quad (49)$$

The error in Eq. (33) can be written as

$$\tilde{\epsilon}_\nu = 1 - \left(e^{-|\alpha_0 + i\eta - \alpha_N|^2} \right)^2. \quad (50)$$

We have $\omega_t t_{\text{rep}} \ll 1$ so, expanding $|\alpha_0 + i\eta - \alpha_N|^2$ to second order and the exponential to first order around zero, we find the expression in Eq. (34).

Acknowledgments

We acknowledge financial support from the Spanish Government via the project PID2024-161371NB-C21 (MCIU/AEI/FEDER, EU) and project TSI-069100-2023-8 (Perte Chip-NextGenerationEU). E.T., acknowledges the Ramón y Cajal (RYC2020-030060-I) research fellowship.

References

- [1] Bruzewicz C D, Chiaverini J, McConnell R and Sage J M 2019 *Applied Physics Reviews* **6** 021314 ISSN 1931-9401 (*Preprint* [1904.04178](#))
- [2] Wang P, Luan C Y, Qiao M, Um M, Zhang J, Wang Y, Yuan X, Gu M, Zhang J and Kim K 2021 *Nature Communications* **12** 233 ISSN 2041-1723
- [3] Harty T P, Allcock D T C, Ballance C J, Guidoni L, Janacek H A, Linke N M, Stacey D N and Lucas D M 2014 *Physical Review Letters* **113** 220501
- [4] Blatt R and Wineland D 2008 *Nature* **453** 1008–1015 ISSN 1476-4687
- [5] An F A, Ransford A, Schaffer A, Sletten L R, Gaebler J, Hostetter J and Vittorini G 2022 *Physical Review Letters* **129** 130501
- [6] Smith M C, Leu A D, Miyanishi K, Gely M F and Lucas D M 2025 *Physical Review Letters* **134** 230601
- [7] Löschnauer C, Mosca Toba J, Hughes A, King S, Weber M, Srinivas R, Matt R, Nourshargh R, Allcock D, Ballance C, Matthiesen C, Malinowski M and Harty T 2025 *PRX Quantum* **6** 040313
- [8] Clark C R, Tinkey H N, Sawyer B C, Meier A M, Burkhardt K A, Seck C M, Shappert C M, Guise N D, Volin C E, Fallek S D, Hayden H T, Rellergert W G and Brown K R 2021 *Physical Review Letters* **127** 130505 ISSN 0031-9007, 1079-7114
- [9] Zhang S, Lu Y, Zhang K, Chen W, Li Y, Zhang J N and Kim K 2020 *Nature Communications* **11** 587 ISSN 2041-1723
- [10] Egan L, Debroy D M, Noel C, Risinger A, Zhu D, Biswas D, Newman M, Li M, Brown K R, Cetina M and Monroe C 2021 *Nature* **598** 281–286 ISSN 1476-4687
- [11] Ryan-Anderson C, Bohnet J G, Lee K, Gresh D, Hankin A, Gaebler J P, Francois D, Chernoguzov A, Lucchetti D, Brown N C, Gatterman T M, Halit S K, Gilmore K, Gerber J A, Neyenhuis B, Hayes D and Stutz R P 2021 *Physical Review X* **11** 041058
- [12] Nguyen N H, Li M, Green A M, Alderete C H, Zhu Y, Zhu D, Brown K R and Linke N M 2021 *Physical Review Applied* **16** 024057 ISSN 2331-7019 (*Preprint* [2104.01205](#))
- [13] Postler L, Butt F, Pogorelov I, Marciniak C D, Heußen S, Blatt R, Schindler P, Rispler M, Müller M and Monz T 2024 *PRX Quantum* **5** 030326
- [14] Monz T, Nigg D, Martinez E A, Brandl M F, Schindler P, Rines R, Wang S X, Chuang I L and Blatt R 2016 *Science (1880 to 2025)* **351** 1068–1070 ISSN 0036-8075
- [15] Debnath S, Linke N M, Figgatt C, Landsman K A, Wright K and Monroe C 2016 *Nature* **536** 63–66 ISSN 1476-4687
- [16] Hempel C, Maier C, Romero J, McClean J, Monz T, Shen H, Jurcevic P, Lanyon B P, Love P, Babbush R, Aspuru-Guzik A, Blatt R and Roos C F 2018 *Physical Review X* **8** 031022
- [17] Liu M, Shaydulin R, Niroula P, DeCross M, Hung S H, Kon W Y, Cervero-Martín E, Chakraborty K, Amer O, Aaronson S, Acharya A, Alexeev Y, Berg K J, Chakrabarti S, Curchod F J, Dreiling J M, Erickson N, Foltz C, Foss-Feig M, Hayes D, Humble T S, Kumar N, Larson J, Lykov D, Mills M, Moses S A, Neyenhuis B, Eloul S, Siegfried P, Walker J, Lim C and Pistoia M 2025 *Nature* **640** 343–348 ISSN 1476-4687
- [18] Figgatt C, Maslov D, Landsman K A, Linke N M, Debnath S and Monroe C 2017 *Nature Communications* **8** 1918 ISSN 2041-1723
- [19] Mølmer K and Sørensen A 1999 *Physical Review Letters* **82** 1835–1838
- [20] Leung P H and Brown K R 2018 *Physical Review A* **98** 032318 ISSN 2469-9926, 2469-9934 (*Preprint* [1808.02555](#))
- [21] Mai X, Zhang L, Yu Q, Zhang J and Lu Y 2025 Scalable entangling gates on ion qubits via structured light addressing (*Preprint* [2506.19535](#))

-
- [22] Choi T, Debnath S, Manning T A, Figgatt C, Gong Z X, Duan L M and Monroe C 2014 *Physical Review Letters* **112** 190502
- [23] Kielpinski D, Monroe C and Wineland D J 2002 *Nature* **417** 709–711 ISSN 1476-4687
- [24] Akhtar M, Bonus F, Lebrun-Gallagher F R, Johnson N I, Siegele-Brown M, Hong S, Hile S J, Kulmiya S A, Weidt S and Hensinger W K 2023 *Nature Communications* **14** 531 ISSN 2041-1723
- [25] Moses S A, Baldwin C H, Allman M S, Ancona R, Ascarrunz L, Barnes C, Bartolotta J, Bjork B, Blanchard P, Bohn M, Bohnet J G, Brown N C, Burdick N Q, Burton W C, Campbell S L, Campora J P, Carron C, Chambers J, Chan J W, Chen Y H, Chernoguzov A, Chertkov E, Colina J, Curtis J P, Daniel R, DeCross M, Deen D, Delaney C, Dreiling J M, Ertsgaard C T, Esposito J, Estey B, Fabrikant M, Figgatt C, Foltz C, Foss-Feig M, Francois D, Gaebler J P, Gatterman T M, Gilbreth C N, Giles J, Glynn E, Hall A, Hankin A M, Hansen A, Hayes D, Higashi B, Hoffman I M, Horning B, Hout J J, Jacobs R, Johansen J, Jones L, Karcz J, Klein T, Lauria P, Lee P, Liefer D, Lu S T, Lucchetti D, Lytle C, Malm A, Matheny M, Mathewson B, Mayer K, Miller D B, Mills M, Neyenhuis B, Nugent L, Olson S, Parks J, Price G N, Price Z, Pugh M, Ransford A, Reed A P, Roman C, Rowe M, Ryan-Anderson C, Sanders S, Sedlacek J, Shevchuk P, Siegfried P, Skripka T, Spaun B, Sprenkle R T, Stutz R P, Swallows M, Tobey R I, Tran A, Tran T, Vogt E, Volin C, Walker J, Zolot A M and Pino J M 2023 *Physical Review X* **13** 041052
- [26] Sterk J D, Coakley H, Goldberg J, Hietala V, Lechtenberg J, McGuinness H, McMurtrey D, Parazzoli L P, Van Der Wall J and Stick D 2022 *npj Quantum Information* **8** 68 ISSN 2056-6387
- [27] Kaushal V, Lekitsch B, Stahl A, Hilder J, Pijn D, Schmiegelow C, Bermudez A, Müller M, Schmidt-Kaler F and Poschinger U 2019 Shuttling-Based Trapped-Ion Quantum Information Processing (*Preprint* [1912.04712](#))
- [28] Main D, Drmota P, Nadlinger D P, Ainley E M, Agrawal A, Nichol B C, Srinivas R, Araneda G and Lucas D M 2025 *Nature* **638** 383–388 ISSN 1476-4687
- [29] Monroe C, Raussendorf R, Ruthven A, Brown K R, Maunz P, Duan L M and Kim J 2014 *Physical Review A* **89** 022317 ISSN 1050-2947, 1094-1622 (*Preprint* [1208.0391](#))
- [30] Knollmann F W, Clements E, Callahan P T, Gehl M, Hunker J D, Mahony T, McConnell R, Swint R, Sorace-Agaskar C, Chuang I L, Chiaverini J and Stick D 2024 *Optica Quantum* **2** 230 ISSN 2837-6714 (*Preprint* [2401.06850](#))
- [31] O'Reilly J, Toh G, Goetting I, Saha S, Shalaev M, Carter A L, Risinger A, Kalakuntla A, Li T, Verma A and Monroe C 2024 *Physical Review Letters* **133** 090802
- [32] Stephenson L J, Nadlinger D P, Nichol B C, An S, Drmota P, Ballance T G, Thirumalai K, Goodwin J F, Lucas D M and Ballance C J 2020 *Physical Review Letters* **124** 110501
- [33] Drmota P, Main D, Nadlinger D P, Nichol B C, Weber M A, Ainley E M, Agrawal A, Srinivas R, Araneda G, Ballance C J and Lucas D M 2023 *Physical Review Letters* **130** 090803
- [34] Pino J M, Dreiling J M, Figgatt C, Gaebler J P, Moses S A, Allman M S, Baldwin C H, Foss-Feig M, Hayes D, Mayer K, Ryan-Anderson C and Neyenhuis B 2021 *Nature* **592** 209–213 ISSN 1476-4687
- [35] García-Ripoll J J, Zoller P and Cirac J I 2003 *Physical Review Letters* **91** 157901
- [36] García-Ripoll J J, Zoller P and Cirac J I 2005 *Physical Review A* **71** 062309
- [37] Duan L M 2004 *Physical Review Letters* **93** 100502
- [38] Mizrahi J, Senko C, Neyenhuis B, Johnson K G, Campbell W C, Conover C W S and Monroe C 2013 *Physical Review Letters* **110** 203001
- [39] Johnson K G, Neyenhuis B, Mizrahi J, Wong-Campos J D and Monroe C 2015 *Physical Review Letters* **115** 213001
-

- [40] Mizrahi J, Neyenhuis B, Johnson K G, Campbell W C, Senko C, Hayes D and Monroe C 2014 *Applied Physics B* **114** 45–61 ISSN 1432-0649
- [41] Bentley C D B, Carvalho A R R and Hope J J 2015 *New Journal of Physics* **17** 103025 ISSN 1367-2630
- [42] Ratcliffe A K, Taylor R L, Hope J J and Carvalho A R R 2018 *Physical Review Letters* **120** 220501
- [43] Mehdi Z, Ratcliffe A K and Hope J J 2021 *Physical Review Research* **3** 013026 ISSN 2643-1564
- [44] Mehdi Z, Ratcliffe A K and Hope J J 2020 *Physical Review A* **102** 012618 ISSN 2469-9926, 2469-9934 (*Preprint* [2005.00367](https://arxiv.org/abs/2005.00367))
- [45] Savill-Brown I, Hope J J, Ratcliffe A K, Vaidya V D, Liu H, Haine S A, Viteri C R and Mehdi Z 2026 *Phys. Rev. Lett.*
- [46] Savill-Brown I, Mehdi Z, Ratcliffe A K, Vaidya V D, Liu H, Haine S A, Viteri C R and Hope J J 2026 *Phys. Rev. A* **113**(5) 052610 URL <https://link.aps.org/doi/10.1103/4thn-7wyf>
- [47] Wong-Campos J D, Moses S A, Johnson K G and Monroe C 2017 *Physical Review Letters* **119** 230501
- [48] Campbell W C, Mizrahi J, Quraishi Q, Senko C, Hayes D, Hucul D, Matsukevich D N, Maunz P and Monroe C 2010 *Physical Review Letters* **105** 090502 ISSN 0031-9007, 1079-7114
- [49] Putnam R, West A D, Campbell W C and Hamilton P 2024 Impulsive Spin-Motion Entanglement for Fast Quantum Computation and Sensing (*Preprint* [2307.11287](https://arxiv.org/abs/2307.11287))
- [50] Johnson K G, Wong-Campos J D, Neyenhuis B, Mizrahi J and Monroe C 2017 *Nature Communications* **8** 697 ISSN 2041-1723
- [51] Metcalf H J and Van Der Straten P 1999 *Laser Cooling and Trapping* Graduate Texts in Contemporary Physics (New York, NY: Springer) ISBN 978-0-387-98728-6 978-1-4612-1470-0
- [52] Hussain M, Heinrich D, Guevara-Bertsch M, Torrontegui E, García-Ripoll J, Roos C and Blatt R 2021 *Physical Review Applied* **15** 024054
- [53] National Academies of Sciences, Engineering, and Medicine 2019 Chapter b: Trapped-ion quantum computers *Quantum Computing: Progress and Prospects* (Washington, DC: The National Academies Press)
- [54] Liu H, Vaidya V D, Galan M G, Ratcliffe A K, Poudel A and Viteri C R 2026 *Phys. Rev. A* **113**(4) 043731 URL <https://link.aps.org/doi/10.1103/972s-wd2q>
- [55] Torrontegui E, Heinrich D, Hussain M I, Blatt R and García-Ripoll J J 2020 *New Journal of Physics* **22** 103024 URL <https://doi.org/10.1088/1367-2630/abbab6>